Domain wall formation and spin reorientation in finite-size magnetic systems

R. M. Fernandes[1,2], H. Westfahl Jr.[1], R. Magalhães-Paniago[1,3] and L. N. Coelho[1,3]

1) Laboratório Nacional de Luz Síncrotron, Caixa Postal 6192, 13084-971, Campinas, SP, Brazil

2) Instituto de Física "Gleb Wataghin", Universidade Estadual de Campinas, 13083-970, Campinas, SP, Brazil *and*

3) Departamento de Física, Universidade Federal de Minas Gerais, 30123-970, Belo Horizonte, MG, Brazil

(Dated: 10th October 2006)

We investigate the formation of stable one-dimensional Néel walls in a ferromagnetic slab with finite thickness and finite width. Taking into account the dipolar, the exchange and the uniaxial anisotropic crystalline field interactions, we derive an approximative analytical self-consistent expression that gives the wall width in terms of ratios between the three different energy scales of the problem. We also show that, even when the crystalline anisotropy does not favour the formation of domain walls, they can yet be formed due to the dipolar interaction and the finiteness of the system. Moreover, using a Stoner-Wohlfarth approach, we study the magnetization reorientation inside the domains under the action of an external magnetic field and obtain the respective hysteresis loops, showing that their shapes change from squared to inclined as the width of the slab varies. Finally, we discuss possible applications of this model to describe qualitatively some recent experimental data on thin films of MnAs grown over GaAs substrates.

PACS numbers: 75.70.Ak ; 75.60.Ch ; 76.60.Es

I. INTRODUCTION

Magnetism in the micro and nanoscales is a source of promising technological advances in a very broad range of interests, from spintronics and quantum computation [1] to biophysics and pharmacology. Nowadays, with the improvement of experimental methods for growth and characterization of magnetic thin films, this particular class of mesoscopic (quasi)two-dimensional systems has been largely investigated [2, 3]. Particularly, one of the properties of such films that has been calling more attention is their magnetic domain structures and their dependence on temperature, film thickness and applied magnetic field [4, 5, 6, 7, 8]. Many of these systems present a competition between a short-range, strong interaction (exchange) and a long-ranged, weak one (dipolar), from which it is expected the emergence of spatially modulated configurations [9, 10]. However, rarely these theoretical models consider possible size effects due to the finiteness of the film width; on the contrary, usually they describe the films as infinite plates, which is fair description of most experimental systems (see, for example, [11, 12, 13, 14]).

One class of magnetic materials that cannot be described as an infinite plate and that has been recently subjected to deep experimental analysis are the thin films of MnAs grown over GaAs substrates (MnAs:GaAs) [8]. In bulk, MnAs exhibits a simultaneous abrupt first-order magnetic/structural transition from a ferromagnetic, hexagonal phase (α phase) to a paramagnetic, orthorhombic one (β phase) [15]. However, MnAs:GaAs films do not show this abrupt transition; conversely, a large region of coexistence between α and β phases arises from $0\,°C$ to $50\,°C$, characterized by the formation of periodic ($\alpha + \beta$) stripes of constant width. The relative witdths of the α and β phases varies with temperature while the total ($\alpha + \beta$) width remains constant [16, 17, 18, 19, 20]. Hence, to understand the domain structure inside each ferromagnetic stripe, and how it varies with temperature, it is important to consider its finite width, specially because in most experimental studies it is of the same order of its thickness.

In this work, we apply the general method of energy minimization already used in other contexts [21, 22, 23] (such as infinite plates, nanoparticles) to study the formation of stable unidimensional domain walls in a slab with finite thickness and finite width. The main purpose of such common procedure is to obtain an expression for the total energy that includes the different interactions contributions. In our case, there are three terms: the exchange term (which tends to unfavour sharp walls); the uniaxial anisotropic crystalline term (which can favour or not the formation of sharp walls, depending on the easy axis of magnetization) and the dipolar term. This last one is rather important in finite systems, as already pointed out by others [10]; we show that, in the system considered here, it is fundamental to form stable walls, specially when the crystalline anisotropy does not favour them. From this energy expression, it is possible to discuss the different solutions for the wall width depending on the three scales of energy involved.

We also generalize the energy expression to include domains whose main magnetization axis is tilted by an angle ϕ with respect to the normal direction to the film. With such expression, it is possible to study how the magnetization is reorientated under the action of an external magnetic field in the direction of the easy axis. This is achieved by calculating theoretical hysteresis curves through a method similar to the one proposed by Stoner and Wohlfarth [24]. This procedure does not take into account nucleation or pinning effects, but only the rotation of the domains and may lead to values of magnetic coercive fields that are not exactly the measured ones. However, as it is a microscopic method, and not a phenomenological one, the main properties predicted are expected to be followed by a variety of experimental systems at least qualitatively.
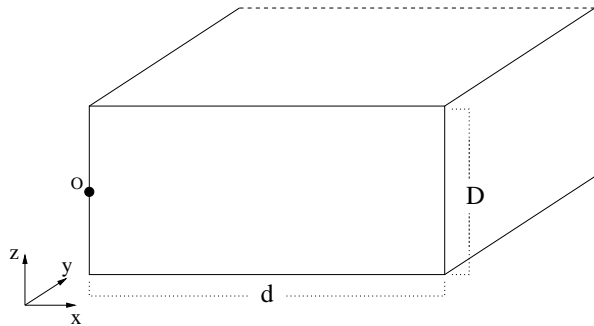
Figure 1: General picture of the coordinate system used to describe the ferromagnetic slab.

Here is an outline of the article: in Section 2, we propose a general expression describing the magnetization corresponding to N domains whose walls width is σ in a slab of thickness D and width d and calculate the corresponding total energy, obtaining an approximative analytical equation. Next, we minimize it with respect to σ and discuss various possible solutions for the wall width depending on the axis of magnetization (if it is the easy or the hard one) and the relationship among the three distinct energy scales. In Section 3, we generalize the previous procedure to inclined domains and discuss the different shapes of the hysteresis loops that describe spin reorientation (i.e., if they are squared or inclined and the values of the coercive fields). Section 4 is devoted to discuss a possible application of the model developed to understand some properties of MnAs thin films (particularly, recent experimental hysteresis curves). Section 5 contains the conclusions and final remarks of the work.

II. ENERGY MINIMIZATION AND WALL WIDTH

Through all this paper, we will use the coordinate system shown in figure 1: the z axis corresponds to the slab thickness (which we shall call D), the x axis, to the slab width (which we shall call d) and the y axis, to the slab length (considered infinite for our purposes). The origin of the axes is located at the middle point of one of the slab's faces, in a way that the x axis points in the direction of the other parallel face. We consider that there is a strong crystalline field that does not allow the magnetization to point in the y direction (xz spin model). This is the case for many experimental systems and, specially, for the MnAs thin films. But we will postpone the discussion about realistic applications of the model until Section 4.

Accordingly, the only kind of unidimensional domain walls that may be formed in this system are Néel walls. Initially, we choose the magnetization to lie along the z direction, in such a way that the walls are along the x direction. Although we are considering an uniaxial

anisotropic system, we will not define yet which of the axis is the easy one. To consider the role of the slab thickness on the formation of these domains, we bound the magnetization to be nonzero only inside it:

$$\vec{M} = [M_x(x)\hat{x} + M_z(x)\hat{z}]\,\theta(D/2 + z)\theta(D/2 - z) \quad (1)$$

where $\theta(x)$ is the Heaviside step function. It can be shown that this formulation would be equivalent to consider sharp domain walls in the upper and lower borders of the slab such that their width is much smaller than the width of the walls along the x direction. As we are concerned with the latter, there is no significant role played by the former in what follows, and we can do $\sigma_z \to 0$.

To investigate the formation of one-dimensional sharp domain walls along the x direction, we propose to study the configuration in which the z component of the magnetization is given by:

$$\begin{aligned} M_z(x) &= M_0 \sum_{i=1}^{N} \frac{(-1)^{i-1}}{2} \left\{ \operatorname{erfc}\left[-\frac{x - d(i-1)/N}{\sqrt{2}\sigma}\right] \right. \\ &\quad \left. -\operatorname{erfc}\left[-\frac{x - di/N}{\sqrt{2}\sigma}\right] \right\}, \end{aligned} \quad (2)$$

where M_0 is the saturation magnetization, $\operatorname{erfc}(x)$ is the complementary error function, N is the number of domains inside the slab and σ corresponds to the wall width along the x axis, which will be varied to minimize the total energy. This model resembles the one used in reference [23]; the choice of using the complementary error function is due to its analytical properties that will allow us to obtain simple expressions for the wall width.

As we are considering a crystalline anisotropy such that $M_y = 0$, we can obtain M_x using the fact that the module of the total magnetization is constant and equal to M_0. Hence, if we meet the condition:

$$\sigma \ll d, \quad (3)$$

then we can obtain a simple approximate expression for M_x in terms of Gaussian functions:

$$M_x(x) = M_0 \sum_{i=1}^{N-1} e^{-\frac{(x - di/N)^2}{2\sigma^2}}. \quad (4)$$

A typical domain configuration described by (2) and (4) is shown in figure 2, where the z and x components of the magnetization are shown as a function of the slab's width.

As we discussed in the previous section, several works [9, 10] have shown that, in systems with competing interactions, a spatially modulated configuration is expected. One may interpret these configurations as "spread" domain walls with sinusoidal domains; however, in this article, we will investigate the formation of sharp walls, for which condition (3) is expected to be satisfied.
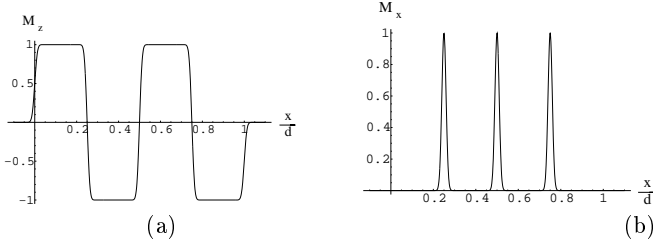
Figure 2: Components (a) M_z and (b) M_x of the magnetization described by (2) and (4) for a four domain configuration along the reduced slab's width x/d.

With the aid of expressions (2) and (4), we can calculate the total energy of a specific domain configuration. However, it is necessary to make an assumption about the microscopic nature of the system if we want to include not only the "macroscopic" terms concerning the dipolar and the crystalline anisotropy interactions, but also the "microscopic" exchange energy. For long wavelengths, one expects that the particular lattice structure (i.e., if it is cubic, hexagonal, etc) will not substantially change the qualitative physical properties derived for another kind of lattice. Hence, to simplify the calculations, we follow [10] and choose the system lattice to be cubic, with lattice parameter a and gyromagnetic factor g. Therefore, it is straightforward to relate the saturation magnetization to the microscopic parameters:

$$M_0 = \frac{g\mu_B}{a^3} \,, \tag{5}$$

where μ_B is the Bohr's magneton. Now, it is possible to obtain the three different energy terms. The exchange term is obtained from the "classical" Heisenberg nearest-neighbours Hamiltonian:

$$
\begin{aligned}
H_{exc} &= -\frac{J}{2} \sum_{\langle ij \rangle} \vec{m}_i \vec{m}_j \\
&= \frac{J}{2a} \int d^3r \left[\left| \vec{\nabla} m_x(\vec{r}) \right|^2 + \left| \vec{\nabla} m_z(\vec{r}) \right|^2 \right] \,,
\end{aligned}
$$

where we moved to the continuum limit of the lattice (see, for instance, [25]) and defined $\vec{m} = \vec{M}/M_0$. Using (1), (2) and (4), we obtain that the exchange energy density is given by:

$$\frac{E_{exc}}{V} = \frac{2J}{a^3} \left[\frac{2N + \pi(N-1)}{8\sqrt{\pi}(d/a)(\sigma/a)} \right] \,. \tag{6}$$

To obtain the dipolar energy, as there are no free currents, we can use equation (see, for instance, the Magnetostatics chapter of [26]):

$$E_{dip} = \frac{1}{2} \int \phi(\vec{r}) \rho(\vec{r}) d^3r \,, \tag{7}$$

where $\rho = -\vec{\nabla} \cdot \vec{M}$ is the effective magnetic charge density and $\phi(\vec{r})$ is the scalar magnetic potential, which satisfies the Poisson equation:

$$\nabla^2 \phi = -4\pi\rho \,.$$

Taking the Fourier transforms of $\rho(\vec{r})$ and $\phi(\vec{r})$, the Poisson equation can be easily solved and equation (7) can be written as:

$$E_{dip} = 2\pi \int \frac{\left| \rho(\vec{k}) \right|^2}{k^2} d^3k \,.$$

Substituting expressions (1), (2) and (4), a straightforward calculation yields, for the magnetostatic energy density:

$$
\begin{aligned}
\frac{E_{dip}}{V} &= \frac{2}{a^3} \left(\frac{g^2 \mu_B^2}{a^3} \right) \left[\left(\frac{\sigma}{d} \right)^2 \epsilon_x \left(\frac{\sigma}{d}, N, p \right) \right. \\
&\quad \left. + \epsilon_z \left(\frac{\sigma}{d}, N, p \right) \right] \,,
\end{aligned} \tag{8}
$$

where $p = d/D$ is the slab's aspect ratio and:

$$
\begin{aligned}
\epsilon_x \left(\frac{\sigma}{d}, N, p \right) &= 2\pi p \int_0^\infty du \frac{e^{-u^2\left(\frac{\sigma}{d}\right)^2}}{u} \left(\frac{u}{p} + e^{-u/p} - 1 \right) \left[1 + \frac{\sin^2 u/2}{\sin^2 u/2N} - 2\cos\left(\frac{u(N-1)}{2N} \right) \frac{\sin u/2}{\sin u/2N} \right] \\
\epsilon_z \left(\frac{\sigma}{d}, N, p \right) &= 4p \int_0^\infty du\, e^{-u^2\left(\frac{\sigma}{d}\right)^2} \frac{e^{-u/2p}}{u^3} \sinh\left(\frac{u}{2p} \right) \tan^2\left(\frac{u}{2N} \right) \left[1 - (-1)^N \cos u \right] \,.
\end{aligned} \tag{9}
$$

Finally, we can calculate the uniaxial crystalline anisotropic term (see, for instance, the Magnetic Anisotropy chapter of [23]):

$$E_{cryst} = -\Delta K \int d^3r\, m_x^2 \,,$$

where ΔK, the anisotropy constant, can be positive or negative, depending if the x axis is the easy ($\Delta K > 0$) or the hard one ($\Delta K < 0$) . Evaluating this calculation, we obtain that the density of anisotropic crystalline energy is:

$$\frac{E_{cryst}}{V} = -2\Delta K \frac{(N-1)\sqrt{\pi}}{2} \left(\frac{\sigma}{d}\right) . \qquad (10)$$

Hence, the total energy is given by:

$$E_{tot} = E_{exc} + E_{dip} + E_{cryst} \qquad (11)$$

As we are assuming condition (3) to be satisfied, we can make a further approximation to obtain a simpler expression for the total energy. Using such condition, we can approximate the exponential $e^{-u^2(\sigma/d)^2}$ in the integrals (9) to 1, as long as we take an appropriate upper limit to them:

$$\epsilon_x \left(\frac{\sigma}{d}, N, p\right) \approx \epsilon_x (0, N, p) \qquad \epsilon_z \left(\frac{\sigma}{d}, N, p\right) \approx \epsilon_z (0, N, p) \qquad (12)$$

This procedure implies in errors of the order of 10% to 20%, if compared to numerical calculations. The choice of the upper limit of the integrals has a small impact on the final result since we are going to apply a self-consistent method in the end of the calculation. Therefore, the qualitative physical properties are still valid in this approximation, and we can minimize (11) as:

$$\begin{aligned} \frac{\partial E_{tot}}{\partial \sigma} &= 0 \\ \frac{\partial^2 E_{tot}}{\partial \sigma^2} &> 0 \,. \end{aligned}$$

To solve these equations, it is convenient to use the following auxiliary variables:

$$\begin{aligned} \left(\frac{\sigma'}{a}\right) &= \left(\frac{\sigma}{a}\right) \left(\frac{J}{g^2\mu_B^2/a^3}\right)^{-1/3} \left(\frac{2N + \pi(N-1)}{64\sqrt{\pi}\,(a/d)\,\epsilon_x(0,N,p)}\right)^{-1/3} \\ \lambda &= \left[\frac{(\Delta K a^3)^3}{J\left(g^2\mu_B^2/a^3\right)^2}\right]^{1/3} \left[\frac{2(N-1)^3\pi^2}{27\left(a\epsilon_x(0,N,p)/d\right)^2(2N+\pi(N-1))}\right]^{1/3} . \end{aligned} \qquad (13)$$

Then, the equation for the domain wall width can be written as:

$$\left(\frac{\sigma'}{a}\right)^3 - 3\lambda\left(\frac{\sigma'}{a}\right)^2 - 4 = 0 . \qquad (14)$$

It is easy to see that the auxiliary variables (13) are just relations between the three different energy scales involved in the system: in σ', there is the ratio between the typical value of the exchange energy and the typical value of the dipolar energy. The other term is just a numerical one and depends only on the ratio a/d, the number of domains N and the aspect ratio p. For thickness of the order of hundreds of lattice parameters, this numerical factor is usually of the order of 10^{-1}, what implies that the relationship between the typical exchange and dipolar energies will determine the order of the wall width. From this, it is clear that when $J \gg g^2\mu_B^2/a^3$ no sharp walls would be formed, as it would be expected.

The parameter λ is a relationship between the three types of energy and can be positive or negative, depending if the x axis is the easy or the hard one, respectively. The numerical factor again depends only on a/d, N and p, and for thickness of the order of hundreds of lattice parameters, it is usually of the order of 10^{-1}.

Let us study the solutions of (14); independently of the sign of λ, equation (14) always has only one positive solution. If $\lambda \geq 0$, this solution is:

$$\begin{aligned} \left(\frac{\sigma'}{a}\right) &= \lambda + \frac{\lambda^2}{\left(1 + \sqrt{1+\lambda^3}\right)^{2/3}} \\ &\quad + \left(1 + \sqrt{1+\lambda^3}\right)^{2/3} , \end{aligned} \qquad (15)$$

while, for $-1 \leq \lambda < 0$, we have:

$$\begin{aligned} \left(\frac{\sigma'}{a}\right) &= \lambda + \frac{\lambda^2}{\left(1 - \sqrt{1+\lambda^3}\right)^{2/3}} \\ &\quad + \left(1 - \sqrt{1+\lambda^3}\right)^{2/3} , \end{aligned} \qquad (16)$$

and in the case where $\lambda < -1$:

$$\left(\frac{\sigma'}{a}\right) = \lambda - 2\lambda \cos\left[\frac{\arg\left(2 + \lambda^3 - 2\sqrt{\lambda^3 + 1}\right)}{3}\right] \qquad (17)$$

In figure 3, we show the graphics of the positive solution as a function of the parameter λ. As expected, when
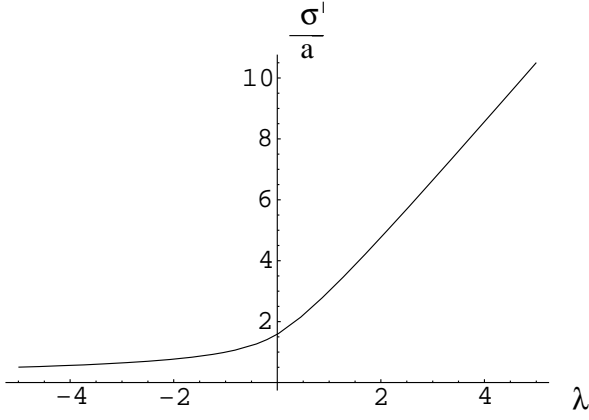
Figure 3: Plot of the general solution σ'/a for the cubic equation (14) as a function of the parameter λ.

λ is negative (magnetization lying on the easy axis), the walls width is smaller than when λ is positive (magnetization lying on the hard axis). We note that even when $\lambda > 0$, i.e., the crystalline anisotropy does not favour the formation of walls, it is possible for the system to be divided in stable domains, as long as the dipolar interaction is large enough compared to both the other two energy scales (as they appear in (13)).

An interesting situation that deserves a deeper analysis is when $0 < \lambda \ll 1$. Such case would occur, for example, if the energy scales satisfied $J \sim g^2\mu_B^2/a^3$ and $g^2\mu_B^2/a^3 \gg \Delta K a^3$. Then, we can expand (15) and obtain:

$$\left(\frac{\sigma'}{a}\right) = 2^{2/3} + \lambda + \mathcal{O}\left(\lambda^2\right),$$

from which we get, to first order in λ:

$$
\begin{aligned}
\left(\frac{\sigma}{a}\right) &= \left(\frac{a^3 J}{g^2\mu_B^2}\right)^{1/3} \left(\frac{2N + \pi(N-1)}{16\sqrt{\pi}\left(\frac{a}{d}\right)\epsilon_x(0,N,p)}\right)^{1/3} \\
&+ \left(\frac{\Delta K\, a^6}{g^2\mu_B^2}\right)\frac{(N-1)\sqrt{\pi}}{\frac{12a}{d}\epsilon_x(0,N,p)}. \quad (18)
\end{aligned}
$$

To avoid numerical problems and reduce the errors concerning the approximation (12), it is useful to transform the general solution for the walls width in a self-consistent equation:

$$\left(\frac{\sigma}{a}\right) = \left(\frac{\sigma'}{a}\right)\left(\frac{a^3 J}{g^2\mu_B^2}\right)^{1/3} \times \quad (19)$$

$$\left(\frac{2N + \pi(N-1)}{64\sqrt{\pi}\frac{a}{d}\,\epsilon_x\left(\frac{\sigma}{d},N,p\right)}\right)^{1/3},$$

in which there is an implicit dependence of σ'/a upon σ. Although this procedure does not give exactly the same result as a numerical method, it prevents one from making further errors due to the integral that appears in $\epsilon_x\left(\frac{\sigma}{d},N,p\right)$.

Finally, it is interesting to study this model in the limit of $d, D \to \infty$, where one expects to recover the result known as Landau-Lifshitz wall (see, for instance [23]). From equation (11), it is clear that the terms referring to the exchange and to the crystalline anisotropy are proportional to d^{-1}. The dipolar term has two parts: ϵ_z, which is due to the surface charge on the upper and lower faces of the slab, goes to zero as $D \to \infty$; ϵ_x is just a finite number for a constant aspect ratio p. Then, making p constant as $d, D \to \infty$, it is clear that this term is proportional to d^{-2} and is negligible if compared to the others. Hence, as pointed in [23], the dipolar energy vanishes in the limit of an "infinite" crystal and domain walls will be formed only if $\Delta K < 0$. Minimizing the energy with respect to σ and putting $N = 2$, we find the result:

$$\left(\frac{\sigma}{a}\right) = 1.06\sqrt{\frac{J}{2\left|\Delta K\right| a^3}},$$

which is just 6% greater than the value of the Landau-Lifshitz wall.

III. THEORETICAL HYSTERESIS LOOPS

We now want to study how this system responds to an external magnetic field applied along the x axis. It is expected that, for strong enough fields, the magnetization will lie along the x axis and will follow the field direction. Our main objective is to determine the qualitative features of the hysteresis curves that would be observed for different slab widths. Therefore, we must generalize our previous model to include rotations of the domains magnetization. Introducing the angle ϕ between the magnetization and the z axis, we can write its components approximately as:

$$M_z(x) = M_0\cos\phi\sum_{i=1}^{N}\frac{(-1)^{i-1}}{2}\left\{\mathrm{erfc}\left[-\frac{x - d(i-1)/N}{\sqrt{2}\sigma}\right] - \mathrm{erfc}\left[-\frac{x - di/N}{\sqrt{2}\sigma}\right]\right\}$$

$$M_x(x) = M_0 (1 - \sin\phi) \sum_{i=1}^{N-1} e^{-\frac{(x-di/N)^2}{2\sigma^2}} + M_0 \frac{\sin\phi}{2} \left\{ \mathrm{erfc}\left[-\frac{x}{\sqrt{2}\sigma}\right] - \mathrm{erfc}\left[-\frac{x-d}{\sqrt{2}\sigma}\right] \right\}, \tag{20}$$

assuming that the condition (3) is satisfied. In what follows, we will consider that the width of the walls is constant, to simplify the calculations. Using the formalism of last section, it is straightforward to conclude that an external magnetic field along the x axis usually will not substantially change the value of the minimum wall width.

It is important to notice that this expression for M_x, (20), as well as the previous one, (4), assumes that the domains are along the positive x direction. Although this feature does not influence any of the results obtained in the last section, it must be taken into account in this one, since we are dealing with spin rotation. If we were to make a complete description of this phenomenon, it would be necessary to include domains in the y direction, otherwise the magnetization inside the walls could never rotate properly. Hence, bidimensional domains would have to be considered, but this is beyond the scope of this article. Therefore, as the domain walls are very small, we

will not treat their rotation, but only the domains rotation. This procedure will then be enough to give us the main qualitative characteristics of the hysteresis loops.

Repeating the procedure of the last section, it is straightforward to calculate the total energy density referring to the configuration (20). We substitute it in the expressions for the exchange, dipolar and crystalline anisotropic energies, obtaining the total energy according to (11). Leaving only the terms proportional to ϕ, we obtain:

$$\frac{E}{2M_0^2} = A(N,d,D)\sin^2\phi \tag{21}$$
$$- \left[B(N,d,D) + \frac{H}{M_0}C\left(N,\frac{\sigma}{d}\right)\right]\sin\phi,$$

where H is the external magnetic field along the x direction and:

$$
\begin{aligned}
A(N,d,D) &= 2\pi p \int_0^\infty \frac{e^{-u^2\left(\frac{\sigma}{d}\right)^2}}{u}\left(\frac{u}{p} + e^{-\frac{u}{p}} - 1\right)\left\{\left(\frac{\sigma}{d}\right)^2\left[1 + \frac{\sin^2 u/2}{\sin^2 u/2N} - 2\cos\left(\frac{u(N-1)}{2N}\right)\frac{\sin\frac{u}{2}}{\sin\frac{u}{2N}}\right]\right. \\
&\quad \left. + \frac{2}{\pi}\frac{\sin^2 u/2}{u^2} - \left(\frac{\sigma}{d}\right)\sqrt{\frac{2}{\pi}}\frac{\sin u/2}{u}\left[\cot\left(\frac{u}{2N}\right)\tan\left(\frac{u}{2}\right) - 1\right]du\right\} \\
&\quad - 4p\int_0^\infty e^{-u^2\left(\frac{\sigma}{d}\right)^2}\frac{e^{-u/2p}}{u^3}\sinh\left(\frac{u}{2p}\right)\tan^2\left(\frac{u}{2N}\right)\left[1 - (-1)^N\cos u\right]du \\
&\quad + \left(\frac{J}{g^2\mu_B^2/a^3}\right)\left[\frac{-2N + \pi(N-1) + 2}{8\sqrt{\pi}(d/a)(\sigma/a)}\right] - \frac{1}{2}\left(\frac{\Delta K a^3}{g^2\mu_B^2/a^3}\right) \\
B(N,d,D) &= 2\pi p\int_0^\infty \frac{e^{-u^2\left(\frac{\sigma}{d}\right)^2}}{u}\left(\frac{u}{p} + e^{-\frac{u}{p}} - 1\right)\left\{\left(\frac{\sigma}{d}\right)^2\left[1 + \frac{\sin^2 u/2}{\sin^2 u/2N} - 2\cos\left(\frac{u(N-1)}{2N}\right)\frac{\sin\frac{u}{2}}{\sin\frac{u}{2N}}\right]\right. \\
&\quad \left. - \left(\frac{\sigma}{d}\right)\frac{1}{2\pi}\frac{\sin u/2}{u}\left[\cot\left(\frac{u}{2N}\right)\tan\left(\frac{u}{2}\right) - 1\right]du\right\} \\
&\quad + 2\left(\frac{J}{g^2\mu_B^2/a^3}\right)\left[\frac{\pi(N-1)}{8\sqrt{\pi}(d/a)(\sigma/a)}\right] \\
C\left(N,\frac{\sigma}{d}\right) &= \frac{1}{2}\left[1 - \left(\frac{\sigma}{d}\right)\sqrt{2\pi}(N-1)\right].
\end{aligned}
\tag{22}
$$

If the condition (3) is satisfied, one can usually make the approximation $C \approx 1/2$, as long as there are few domains inside the slab.

As we did not consider the terms independent of ϕ in the total energy expression (21), we note that the energy of the configuration studied in the previous section, cor-

responding to $\phi = 0$, would be $E = 0$. Indeed, the terms that appear in (21) are a combination of the exchange, dipolar and crystalline anisotropic energies referring to the components of the magnetization (20) that are not parallel to the z direction. It is clear that the total energy will be non-zero only for configurations in which the

the magnetization is tilted by some angle with respect to the z axis.

Now, it is possible to apply a procedure similar to the one developed by Stoner and Wohlfarth [24] to analyze the spin reorientation in the presence of a magnetic field. Minimizing equation (22) with respect to ϕ leads us to

$$\frac{\partial E}{\partial \phi} = 2A\sin\phi\cos\phi - \left(B + \frac{H}{M_0}C\right)\cos\phi \quad (23)$$
$$= 0,$$

while the second derivative is given by

$$\frac{\partial^2 E}{\partial\phi^2} = 2A\cos 2\phi + \left(B + \frac{H}{M_0}C\right)\sin\phi. \quad (24)$$

Equation (23) has two possible solutions: the first one refers to the two possible orientations for which the magnetization lies on the x axis:

$$\cos\phi_1 = 0 \Rightarrow \phi_1 = \pm\frac{\pi}{2}, \quad (25)$$

and is a minimum as long as:

$$-2A + \left(B + \frac{H}{M_0}C\right) \geq 0, \quad (26)$$

if $\phi_1 = \pi/2$, or:

$$-2A - \left(B + \frac{H}{M_0}C\right) \geq 0, \quad (27)$$

if $\phi_1 = -\pi/2$. The second solution is:

$$\phi_2 = \arcsin\left(\frac{B + \frac{H}{M_0}C}{2A}\right), \quad (28)$$

and it is a minimum for

$$2A \geq \frac{\left(B + \frac{H}{M_0}C\right)^2}{2A}. \quad (29)$$

Therefore, we can build a procedure to trace the upper curve of the hysteresis loop. Applying a strong enough

positive magnetic field, the magnetization will lie along the positive x direction, since $\phi_1 = \pi/2$ will be the global minimum. As H diminishes, and eventually becomes negative, condition (26), at some moment, will no more be satisfied and two options will raise. If $A \leq 0$, while condition (29) will never be satisfied, condition (27) will be, and the system will jump to the configuration in which the magnetization lies along the negative x direction ($\phi = -\pi/2$). Hence, the upper curve of the hysteresis loop has the shape of an abrupt step when $A \leq 0$. The remanent magnetization along the x axis is simply

$$M_r = M_0, \quad (30)$$

and the coercive field is given by:

$$H_c = -M_0\left(\frac{B - 2A}{C}\right). \quad (31)$$

However, if $A > 0$, other stable states will raise before $\phi = -\pi/2$ is reached, since condition (29) is satisfied. Then, the system jumps continuously from minimum to minimum, as none of them can be a metastable state. This behaviour continues until H is strong enough to not satisfy condition (29) anymore. Hence, condition (27) is satisfied and the magnetization lies along the negative x direction. In this case, in which $A > 0$, the upper curve has the shape of an inclined step. The remanent magnetization along the x axis is given by:

$$M_r = \begin{cases} M_0 & \text{, if } B > 2A \\ M_0\left(\frac{B}{2A}\right) & \text{, otherwise} \end{cases} \quad (32)$$

and the coercive field by

$$H_c = -M_0\left(\frac{B}{2C}\right). \quad (33)$$

To obtain the lower curve of the hysteresis loop, we have to perform a slight modification. As previously explained, the configuration considered assumes that the domain walls are along the positive x direction. However, after the magnetization is reoriented, we must consider a new configuration in which the domain walls are along the negative x direction, so we avoid additional errors for not considering domains along the y direction. Hence, we take:

$$M_x(x) = M_0\left(-1 - \sin\phi\right)\sum_{i=1}^{N-1} e^{-\frac{(x - di/N)^2}{2\sigma^2}} + M_0\frac{\sin\phi}{2}\left\{\mathrm{erfc}\left[-\frac{x}{\sqrt{2}\sigma}\right] - \mathrm{erfc}\left[-\frac{x - d}{\sqrt{2}\sigma}\right]\right\}. \quad (34)$$

Equation (21) is then replaced by

$$\frac{E}{2M_0^2} = A\left(N, d, D\right)\sin^2\phi + \left[B\left(N, d, D\right) - \frac{H}{M_0}C\left(N, \frac{\sigma}{d}\right)\right]\sin\phi. \tag{35}$$

Following the same procedure as before, we obtain that the lower curve has the same shape of the upper one, and the remanent magnetization along the x axis and the coercive field are symmetrical to the ones presented previously, (30)-(33).

Therefore, we conclude that, if $A \leq 0$, the hysteresis loop is squared, the remanent magnetization is M_0 and the coercive field is given by (31). If $A > 0$, instead, the hysteresis loop is inclined, the remanent magnetization is given by (32) and the coercive field by (33).

IV.   APPLICATION TO MnAs : GaAs

Several works were done regarding magnetic properties of MnAs thin films grown over GaAs substrates. Here we will discuss possible applications of our model to the experimental hysteresis loops recently obtained [27, 28, 29]. To make correspondence between our model and the real system, it is useful to identify the following crystallographic directions of MnAs to the axis considered in figure 1: $[\bar{1}\bar{1}20] = x$, $[0001] = y$ and $[\bar{1}100] = z$.

First of all, let us outline the parameters of the MnAs thin films that we will use in our calculations. As measured in [30], the anisotropy constants associated to the z and to the x axis are, respectively, $K_z = 7 \cdot 10^6\,\mathrm{erg/cm^3}$ and $K_x = 7.4 \cdot 10^6\,\mathrm{erg/cm^3}$. Hence, the x axis is the easy one, and we can use $\Delta K = 0.4 \cdot 10^6\,\mathrm{erg/cm^3}$. From the crystalline structure of MnAs [8],which is in fact hexagonal, we estimate the value of the equivalent cubic lattice parameter to be $a = 4\,\mathrm{A}$. The gyromagnetic factor was estimated as $g = 4.5$, from which we obtain a magnetization of $M_0 = 0.65 \cdot 10^6\,\mathrm{A/m}$, that is very close to the experimental value measured of $M_0 = 0.67 \cdot 10^6\,\mathrm{A/m}$ [31]. As we are interested in orders of magnitude, we estimate $J = 4.5\,\mathrm{meV}$ from the Curie temperature of MnAs. Finally, as these films have constant thickness, we take the fixed value $D = 130\,\mathrm{nm}$, which is the thickness of the sample used in [29] and of the same order of magnitude of usual samples.

Magnetic Force Microscopy (MFM) images of MnAs:GaAs films have suggested that [29, 32], as the temperature rises in the coexistence region (implying in smaller widths of the ferromagnetic stripe), the system undergoes a transition from a configuration in which the magnetization lies along the easy x axis to another one in which it lies along the growth axis (the hard z axis) and is divided in three domains. Let us verify the predic-
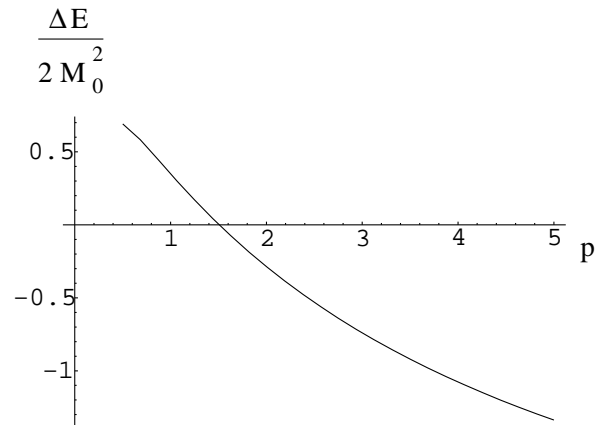

Figure 4: Plot of the energy difference between the configuration in which the magnetization lies along the x axis and the one in which there are three domains lying along the z axis as a function of the aspect ratio p of the ferromagnetic stripe.

tions of our model for these situation: substituting the experimental parameters of MnAs in the self-consistent equation (19) for $N = 3$ domains, we obtain that the domain walls are stable and that their width is given by $\sigma = 3.8a$. The solution to the cubic equation (14) used was (18), since the experimental parameters of MnAs imply $\lambda \ll 1$. A numerical calculation in fact gives a width of about $5a$, what confirms our expectations that the approximative self-consistent method gives errors less than 20%.

Using equation (21), it is possible to obtain the energy difference between the two configurations seen in the MFM images. In figure 4, we show the plot of this difference as a function of the aspect ratio p and notice that there is a transition at $p_c \approx 1.5$. The measurements realized by Coelho $et.$ $al.$ [29] suggest that this transition takes place around $p_c \approx 2.9$. However, as mentioned previously, we do not take into account the domains along the y direction or the inter-stripe interaction, a feature always observed in the MFM images. This seems to be particular important not only to provide more precise values for p_c but also to ensure that the most stable configuration has 3 domains. Without taking into account such features, our model would predict also transitions to $N > 3$ domain configurations before the one at $N = 3$, what is not observed in the MFM images. Hence, we can only predict a qualitative behaviour of the real system.
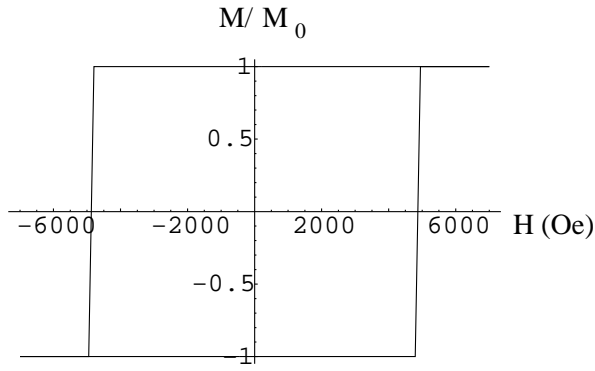
Figure 5: Plot of the hysteresis loop predicted by the model for $p = 1.9$. The vertical axis represents the relative magnetization M/M_0 along the x axis and the horizontal axis represents the external magnetic field H applied in the x direction in Oe.
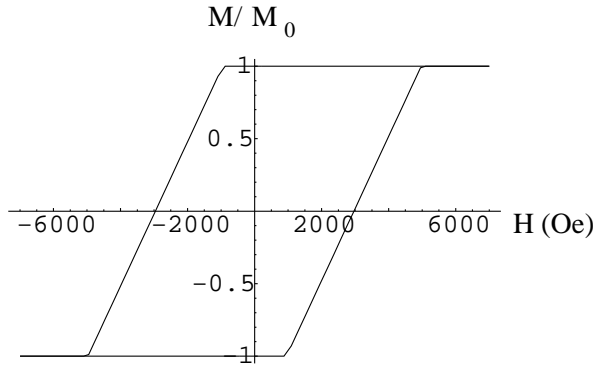

Figure 6: Plot of the hysteresis loop predicted by the model for $p = 1.7$. The vertical axis represents the relative magnetization M/M_0 along the x axis and the horizontal axis represents the external magnetic field H applied in the x direction in Oe.
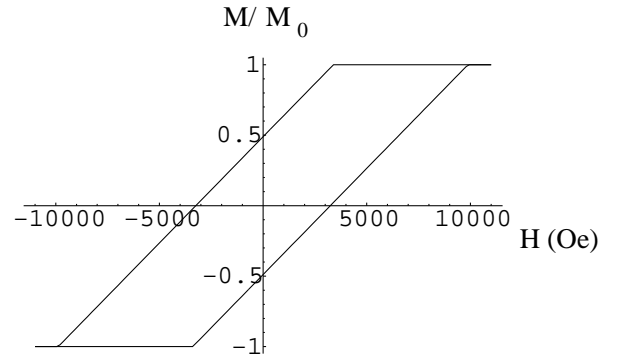

Figure 7: Plot of the hysteresis loop predicted by the model for $p = 1.5$. The vertical axis represents the relative magnetization M/M_0 along the x axis and the horizontal axis represents the external magnetic field H applied in the x direction in Oe.
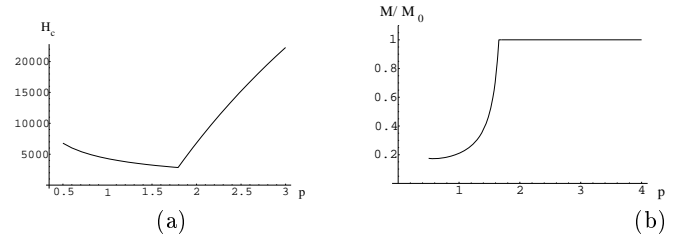

Figure 8: Plot of the (a) modulus H_c of the coercive field (in Oe) and (b) of the relative remanent magnetization M/M_0 along the x axis as a function of the aspect ratio p of the ferromagnetic stripe.

It is interesting to plot the theoretical hysteresis loops predicted by our model for a $N = 3$ domain configuration with the MnAs experimental parameters. Applying the procedure developed in the previous section, we see that $B > 0$ for any value of the aspect ratio p and A is negative until $p \approx 1.8$, where it becomes positive. Hence, it is expected that the hysteresis shape is squared until $p \approx 1.8$, where it becomes inclined. For $1.65 < p < 1.8$, the remanent magnetization is expected to be yet M_0, and only for $p < 1.65$ it will start to decrease. Figures 5, 6 and 7 show the three different possible shapes of the hysteresis loops, according to the procedure of the last section.

It is worth to notice that hysteresis loops of shapes similar to figures 7 and 6 (but more rounded) were observed in [28] and [29], respectively, while shapes like the one in figure 4 were seen in both of them. Coelho *et. al.* showed that the change in the shape of the hysteresis loops occurs for $p \approx 2.9$, which is not too far from our prediction ($p \approx 1.8$). However, our coercive fields are one order of magnitude greater than the values obtained by both [29] and [28]. It is interesting to notice that simulations performed by Engel-Herbert *et. al.* [28] considering other configurations and other methods led to the same order of magnitude for the coercive fields than our model. The graphics of the coercive field and the remanent magnetization predicted by our model are shown in figure 8, where it is easy to verify the paths for the transitions among the three different types of hysteresis loops pointed before.

Finally, we point out that, in [27], Takagaki *et. al.* found a hysteresis loop similar to the squared one (figure 5) for MnAs thin films and another similar to the inclined one (figure 6) (but more rounded, again) for disks of MnAs fabricated from thin films. It is evident that our model cannot be applied to disks (in such case, there is the possibility of more complex configurations, like vortices, for example), but it may give a hint about their physical behaviour.

V. CONCLUSIONS

In this article, we have shown, using an approximative analytical self-consistent equation, that multiple-domains configurations with sharp walls in a ferromagnetic slab can be stable. We arrived at ratios among the three typical magnetic energy scales of the system (exchange, dipolar and crystalline anisotropic) that can determine the stability of these configurations and also give the order of magnitude for the walls width. Although the approximations done to achieve these equations introduces imprecision on the predictions of the model, they do not significantly change the orders of magnitude involved. Moreover, this model shows that, even when the crystalline anisotropy prefers spread walls, the dipolar interaction can compensate it to form sharp ones. In what concerns thin films of MnAs grown over GaAs substrates, which could be an observable realization of our model, we corroborated the suggestions based on MFM images that predicts the formation of three-domain configurations along the hard axis, for temperatures above $25\,^{\circ}$C. The transition between this state and the configuration in which the magnetization lies completely along the easy axis was also predicted, but the value of the film aspect ratio for which this transition occurs was far from the experimental one.

In addition, we compared the hysteresis loops that appears when an external magnetic field is applied along the easy axis direction for such three-domain configurations. Qualitatively, we obtained, using an approach similar to Stoner and Wohlfarth [24], all the three shapes of loops observed in the literature (squared, inclined with large remanent magnetization and inclined with small remanent magnetization). The main differences are that the inclined loops measured experimentally are more rounded than ours and that the experimental coercive fields are one order of magnitude smaller.

Several factors help us to understand why all these differences between the predictions of the model and the experimental measurements occur. Firstly, the simple model we used here does not consider features that are essential in the MnAs:GaAs real system, like the modulation along the y direction and the inter-stripe dipolar interaction. To include these features, a more sophisticated model with bidimensional domains and topological defects would be necessary. Moreover, in what concerns the hysteresis loops, the Stoner-Wohlfarth method deals only with the collective spin rotation, and does not take into account nucleation or pinning, which can be responsible for the rounded shape of the curves and the smaller coercive fields observed in the experiments. As already pointed out in [28], due to the lack of complete knowledge about the exact geometrical forms of the ferromagnetic stripes, the materials inhomogeneities (that can induce nucleation) and the correct microscopic parameters, we cannot expect an exact reproduction of the experimental hysteresis loops. Nonetheless the qualitative physical properties predicted here give an insight for a more complete understanding of the complex domain structure of systems like MnAs:GaAs films.

[1] S. A. Wolf, D. D. Awaschalom, R. A. Buhrman, J. M. Daughton, S. von Molnas, M. L. Roukes, A. Y. Chtchelkanova, D. M. Treger. Science **294**, 1488 (1994)

[2] T. L. Jones and D. Venus, Surf. Sci. **302**, 126 (1994)

[3] M. Prutton, *Introduction to Surface Physics*, Clarendon, Oxford (1994)

[4] D. P. Pappas, K. -P. Kamper and H. Hopster, Phys. Rev. Lett. **6**4, 3179 (1990)

[5] R. Allenspach, M. Stampanoni and A. Bischof, Phys. Rev. Lett. **65**, 3344 (1990)

[6] R. Allenspach and A. Bischof, Phys. Rev. Lett. **69**, 3385 (1992)

[7] A. Berger and H. Hopster, Phys. Rev. Lett. **76**, 519 (1996)

[8] A. K. Das, C. Pampuch, A. Ney, T. Hesjedal, L. Daweritz, R. Koch and K. H. Ploog, Phys. Rev. Lett. **91**, 087203 (2003)

[9] M. Seul and D. Andelman, Science **267**, 476 (1995)

[10] T. Garel and S. Doniach, Phys. Rev. B **26**, 325 (1982)

[11] J. A. Cape and G. W. Lehman, J. Appl. Phys. **42**, 5732 (1971)

[12] Ar. Abanov, V. Kalatsky, V. L. Pokrovsky and W. M. Saslow, Phys. Rev. B **51**, 1023 (1995)

[13] P. J. Jensen and K. H. Bennemann, Phys. Rev. B **52**, 16012 (1995)

[14] I. Booth, A. B. MacIsaac, J. P. Whitehead and K. De'Bell, Phys. Rev. Lett. **75**, 950 (1995)

[15] C. P. Bean and D. S. Rodbell, Phys. Rev. **126**, 104 (1962)

[16] R. Engel-Herbert, J. Mohanty, A. Ney, T. Hesjedal, L. Daweritz and K. H. Ploog, Appl. Phys. Lett. **84**, 1132, (2004)

[17] V. M. Kaganer, B. Jenichen, F. Schippan, W. Braun, L. Daweritz and K. H. Ploog, Phys. Rev. B **66**, 045305 (2002)

[18] A. Ney, T. Hesjedal, C. Pampuch, A. K. Das, L. Daweritz, R. Koch, K. H. Ploog, T. Tolinski, J. Lindner, K. Lenz and K. Baberschke, Phys. Rev. B **69**, 081306 (2004)

[19] R. Magalhães-Paniago, L. N. Coelho, B. R. A. Neves, H. Westfahl, F. Iikawa, L. Daweritz, C. Spezzani and M. Sacchi, Appl. Phys. Lett. **86**, 053112 (2005)

[20] F. Iikawa, M. Knobel, P. V. Santos, C. Adriano, O. D. D. Couto, M. J. S. P. Brasil, C. Giles, R. Magalhães-Paniago and L. Daweritz, Phys. Rev. B **71**, 045319 (2005)

[21] C. Kittel, Rev. Mod. Phys. **21**, 541 (1949)

[22] Z. Málek and V. Kambersky, Czech. J. Phys. **21**, 416

(1958)

[23] A. Aharoni, *Introduction to the Theory of Ferromagnetism*, Claredon, Oxford (1996)

[24] E. C. Stoner and E. P. Wohlfarth, Phil. Trans. R. Soc. London **A240**, 599 (1948), reprinted IEEE Trans. Magnetics **27**, 3475 (1991)

[25] J. W. Negele and H. Orland, *Quantum Many-Particle Systems*, Advanced Book Classics, Perseus, USA (1998)

[26] J. D. Jackson, *Classical Electrodynamics*, John Wiley and Sons, USA (1998)

[27] Y. Takagaki, C. Herrmann, E. Wiebicke, J. Herfort, L. Daweritz and K. H. Ploog, Appl. Phys. Lett. **88**, 032504 (2006)

[28] R. Engel-Herbert, T. Hesjedal, J. Mohanty, D. M. Schaadt and K. H. Ploog, Phys. Rev. B **73**, 104441 (2006)

[29] L. N. Coelho, R. Magalhães-Paniago, B. R. A. Neves, F. C. Vicentin, H. Westfahl, R. M. Fernandes, F. Iikawa, L. Daweritz, C. Spezzani and M. Sacchi, *to be published* (2006)

[30] J. Lindner, T. Tolinski, K. Lenz, E. Kosubek, H. Wende, K. Baberschke, A. Ney, T. Hesjedal, C. Pampuch, R. Koch, L. Daweritz and K. H. Ploog, J. Magn. Magn. Mater. **277**, 159 (2004)

[31] F. Schippan, G. Behme, L. Daweritz, K. H. Ploog, B. Dennis, K. -U. Neumann and K. R. A. Ziebeck, J. Appl. Phys. **88**, 2766 (2000)

[32] T. Plake, T. Hesjedal, J. Mohanty, M. Kastner, L. Daweritz and K. H. Ploog, Appl. Phys. Lett. **84**, 1132 (2004)